

# Downlink Clustering-Based Scheduling of IRS-Assisted Communications With Reconfiguration Constraints

Alberto Rech, Leonardo Badia, Stefano Tomasin, Matteo Pagin,  
Marco Giordani, Jonathan Gambini, Michele Zorzi

**Abstract**—Intelligent reflecting surfaces (IRSs) are being widely investigated as a potential low-cost and energy-efficient alternative to active relays for improving coverage in next-generation cellular networks. However, technical constraints in the configuration of IRSs should be taken into account in the design of scheduling solutions and the assessment of their performance. To this end, we examine an IRS-assisted time division multiple access (TDMA) cellular network where the reconfiguration of the IRS incurs a communication cost; thus, we aim at limiting the number of reconfigurations over time. Along these lines, we propose a clustering-based heuristic scheduling scheme that maximizes the cell sum capacity, subject to a fixed number of reconfigurations within a TDMA frame. First, the best configuration of each user equipment (UE), in terms of joint beamforming and optimal IRS configuration, is determined using an iterative algorithm. Then, we propose different clustering techniques to divide the UEs into subsets sharing the same sub-optimal IRS configuration, derived through distance- and capacity-based algorithms. Finally, UEs within the same cluster are scheduled accordingly. We provide extensive numerical results for different propagation scenarios, IRS sizes, and phase shifters quantization constraints, showing the effectiveness of our approach in supporting multi-user IRS systems with practical constraints.

**Index Terms**—Fifth generation (5G); Intelligent Reflecting Surfaces (IRS); millimeter wave (mmWave) communication; multiple access; scheduling; clustering; optimization.

## I. INTRODUCTION

The ever-increasing growth of mobile traffic has called both academia and industry to identify and develop solutions for extending the radio spectrum beyond the crowded sub-6 GHz bands. As a result, the millimeter wave (mmWave) band has been included in the used bands for cellular communications in the latest releases of the 3rd Generation Partnership Project (3GPP) standard, namely fifth-generation (5G) New Radio (NR) [2]. Moreover, the use of Terahertz (THz) frequencies is being investigated as a possible key technology enabler for sixth-generation (6G) networks as well [3].

Alberto Rech, Leonardo Badia, Stefano Tomasin, Matteo Pagin, Marco Giordani, and Michele Zorzi are with the Department of Information Engineering, University of Padova, Italy. Jonathan Gambini is with the Milan Research Center, HUAWEI, Italy. Corresponding author: A. Rech (email: alberto.rech.2@phd.unipd.it).

This work was supported in part by the European Union through the Italian National Recovery and Resilience Plan (NRRP) of NextGenerationEU, partnership on “Telecommunications of the Future” (Program “RESTART”) under Grant PE0000001. Part of this paper has been presented at the IEEE Wireless Communications and Networking Conference (WCNC), [1].

However, transmissions in the mmWave and THz bands are subject to challenging propagation conditions, mainly due to severe path loss and susceptibility to blockages [4]. To mitigate these limitations, a possible solution is to densify the network, thus reducing the cell radius. Unfortunately, this approach was shown to be infeasible for network operators, since trenching and deploying the necessary fiber backhaul links usually represents an excessive financial and logistical hurdle [5], [6]. This issue is exacerbated in remote areas, where the limited access to electrical power and the lower density of user equipments (UEs) further complicates dense network deployments from a business standpoint [7], [8]. Even worse, network densification will also inevitably increase carbon emissions due to base stations management operations, with serious environmental concerns.

To solve these issues, the research community has explored new technologies to improve network coverage, for example using integrated access and backhaul (IAB) nodes, as also approved by the 3GPP as part of 5G NR specifications for Rel-16 [9]. In particular, IAB allows base stations, or next generation Node Bases (gNBs) in 5G NR parlance, to establish wireless (rather than traditional fiber-like) backhaul links, possibly through multiple hops, to a donor, thus reducing deployment costs [10]. Still, IAB involves complex signal processing and saturation of the available resources, and may be costly and energy-consuming for network operators.

In light of this, intelligent reflecting surfaces (IRSs) are being investigated as possible solutions to overcome the harsh propagation conditions shown by mmWave and THz bands in a cost- and energy-efficient manner [11]. Specifically, IRSs are meta-surfaces whose radiating elements can *passively* tune the phase shift of impinging signals to favorably alter an electromagnetic field towards an intended destination. Therefore, they can be configured to beamform the reflected signal virtually in any direction, hence acting as relay to improve the signal quality without an active (power-consuming) amplification [12].

*Prior work.* Despite the substantial research hype, most recent studies on IRSs rely on strong assumptions that do not match actual real-world deployments. Specifically, a significant body of literature is based on the assumption that IRSs establish an ideal (i.e., fiber-like) control channel with the base station [13]–[16]. Instead, actual deployments are expected to feature a wireless, i.e., error-prone, IRS control channel, possibly implemented with low-cost technologies [17], [18].

This will introduce constraints on the IRS reconfiguration period, which needs to be synchronized with the base station to beamform the signal towards the UE served during the specific time slot [11], a similar research problem than scheduling in cellular networks.

In this perspective, IRS-assisted downlink scheduling solutions have been widely studied in different domains, each with its own theoretical constraints. For example, in multi-user scheduling based on orthogonal frequency-division multiple access (OFDMA), due to the lack of frequency-selective passive beamforming capabilities at the IRS, only one set of reflection coefficients can be designed for adapting to all the users assigned to the same time slot. In this context, dynamic optimization schemes, wherein the IRS configurations are adjusted over each time slot, have been studied in [19], [20]. Moreover, a user scheduling method based on graph neural networks, able to jointly optimize the IRS configuration and the gNB beamforming in downlink networks, was recently presented in [21]. Similarly, the authors in [22]–[24] evaluated the performance of several non-orthogonal downlink scheduling methods, including non-orthogonal multiple access (NOMA) and rate-splitting multiple access (RSMA).

Nevertheless, early IRS control circuitry prototypes, which have a low power consumption (i.e., in the order of hundreds of mW), exhibit non-negligible phase-shifts reconfiguration time [25], which poses additional constraints. Moreover, the expected large number of elements of an IRS will also increase the overhead (in terms of time and energy), as investigated in [26]–[28]. Thus, a constraint on the number of reconfigurations (and relative period) should be accounted for to ensure system synchronization. In this regard, it is of interest to (i) investigate the level of performance degradation experienced by IRS-assisted systems when considering practical constraints, including limitations in the number of reconfigurations, and (ii) design algorithms that can mitigate these limitations.

The problem at hand can be seen as a bipartite matching [29] between users and IRS parameter configurations, made more complex by limitations in the number and the dimensionality of the usable configurations. In general, such problems of assigning resources in a potentially large network are not new to cellular scheduling [30], and the extension to multidimensional cases is common for multi-user diversity or coordinated multipoint (CoMP) [31]. Standard approaches trying to minimize the computational complexity involve the identification and assignment of efficient patterns that can be repeated [32], [33], as well as the dynamic and distributed creation of clusters that the users join to receive the same kind of resource allocation [34], [35].

*Contributions.* Based on the above introduction, in this paper we propose a time division multiple access (TDMA) scheduling policy for downlink cellular transmissions based on clustering algorithms, to maximize the sum capacity in IRS-assisted network deployments with practical constraints. Notably, we assume a fixed maximum number of IRS reconfigurations within a time frame, and aim at optimizing both the reconfiguration time and the resulting IRS configuration(s). The limit on the number of reconfigurations sets a simple

constraint on the overhead entailed by the control of the IRS. Our contributions can be summarized as follows:

- We formalize an optimization problem to determine the optimal IRS configuration(s) to maximize the sum capacity. Specifically, we partition the UEs into disjoint groups, and propose an algorithm that iteratively optimizes the IRS configuration for each group, as well as the relative beamformers to be used for transmission.
- We convert the sum capacity problem into a clustering problem to determine the optimal set of groups, or clusters, for the UEs based on their channel characteristics. Accordingly, we design clustering algorithms for the UEs, such that all UEs in the same cluster will adopt the same IRS configuration. The goal is to minimize the capacity loss associated with a sub-optimal IRS configuration for each UE in the cluster, for promoting communication efficiency and reducing the overhead. We investigate two clustering techniques:
  - (i) distance-based clustering, which adjusts the cluster configuration based on the distance with the optimal IRS configuration of each UE in the cluster;
  - (ii) capacity-based clustering, which adjusts the cluster configuration to maximize the sum capacity and/or the user fairness. Specifically, we propose three clustering algorithms. The first, named capacity-weighted clustering (CWC), iteratively adjusts the clusters' centroids weighting the points in each cluster by the capacity achieved by each UE in the cluster, therefore favoring the best users and maximizing the sum capacity. The second, named one-shot capacity-based clustering (OSCBC), is a low-complexity approach wherein the centroids are simply the optimal configurations of the UEs experiencing the highest signal-to-noise-ratio (SNR) in each cluster, without considering the impact of the remaining UEs. Finally, inverse capacity-weighted clustering (ICWC) promotes fairness among the UEs by weighting the points in the clusters by the inverse of the UEs' achievable rate.
- We compare via simulation the performance of the distance- and capacity-based clustering in different IRS-assisted scenarios. Extensive numerical results show that there exists a trade-off between the achievable sum capacity and fairness, even though capacity-based clustering techniques can guarantee satisfactory performance, despite some reconfiguration constraints. Also, we demonstrate that scheduling based on clustering can reduce by 50% the number of IRS reconfigurations, thus promoting energy efficiency, in view of minor degradation in terms of sum rate.
- With respect to [1], we introduce new capacity-based clustering strategies to improve fairness, and provide more extensive numerical results to demonstrate the scalability of the proposed solutions as a function of the density of UEs and the IRS size. Moreover, we evaluate the performance of the proposed scheduling strategies considering realistic IRS network constraints, including the quantization of phase shifts, and for different channel

propagation conditions. Furthermore, we provide additional results in terms of the computational complexity of the proposed distance- and capacity-based clustering algorithms, as well as in terms of fairness.

*Organization.* The rest of the paper is organized as follows. In Section II we introduce the system model and present the sum capacity optimization problem. In Section III we describe the scheduling framework, while in Sections IV and V we present our proposed distance-based and capacity-based clustering algorithms, respectively. In Section VI we show our numerical results, and compare the different scheduling and clustering solutions. Finally, Section VII draws the main conclusions.

*Notation.* Scalars are denoted by italic letters; vectors and matrices by boldface lowercase and uppercase letters, respectively; sets are denoted by calligraphic uppercase letters.  $\text{diag}(\mathbf{a})$  indicates a square diagonal matrix with the elements of  $\mathbf{a}$  on the principal diagonal.  $\mathbf{A}^T$  and  $\mathbf{A}^\dagger$  denote the transpose and the conjugate transpose of matrix  $\mathbf{A}$ , respectively.  $[\mathbf{A}]_{k\ell}$  denotes the scalar value in the  $k$ -th row and  $\ell$ -th column of matrix  $\mathbf{A}$ , while  $\mathbf{a}_k$  denotes the  $k$ -th element of vector  $[\mathbf{a}]$ . The imaginary unit is denoted as  $j = \sqrt{-1}$ , and  $\angle a$  denotes the phase of  $a \in \mathbb{C}$ . Finally,  $\mathbb{E}[\cdot]$  denotes statistical expectation.

## II. SYSTEM MODEL

We consider downlink data transmissions for the multi-user multiple input multiple output (MIMO) communication system shown in Fig. 1, wherein the transmission from the gNB to the  $K$  UEs is assisted by an IRS. The gNB and the UEs are equipped with  $N_g$  and  $N_U$  antennas, respectively. We assume that the direct link between the gNB and the UEs is unavailable due to a deep blockage. As a consequence, the gNB transmits signals to the UEs by exploiting the virtual link offered by the IRS. Time is divided into frames, each split into  $K$  slots, and each UE is served exactly once in a frame.

### A. IRS Model

Each of the  $N_I$  elements of the IRS acts as an omnidirectional antenna unit that reflects the impinging electromagnetic field by introducing a tunable phase shift on the baseband-equivalent signal. We denote as  $\phi_n = e^{j\theta_n}$  the reflection coefficient of the  $n$ -th IRS element, where  $\theta_n \in \mathcal{P}_\theta$  is the induced phase shift, and  $\mathcal{P}_\theta$  is the set of possible phase shifts.

Recent works argue that continuous phase shifts are hardly implementable in practice [36]. Therefore, we consider both continuous and quantized phase shifts. While in the former case the set of possible phase shifts is simply  $\mathcal{P}_\theta = [-\pi, \pi)$ , in the latter we have

$$\mathcal{P}_\theta = \left\{ 0, \frac{2\pi}{2^b}, \dots, \frac{2\pi(2^b - 1)}{2^b} \right\}, \quad (1)$$

where  $b > 0$  is the number of bits employed to control the quantized phase shifts.

We denote with  $\mathbf{H} \in \mathbb{C}^{N_I \times N_g}$  the channel matrix between the IRS and the gNB, and with  $\mathbf{G}_k \in \mathbb{C}^{N_U \times N_I}$  the channel matrix of the link between the IRS and UE  $k$ , respectively. We consider single-stream transmissions, with  $\mathbf{w}_k \in \mathbb{C}^{N_g \times 1}$  and

$\mathbf{v}_k \in \mathbb{C}^{N_U \times 1}$  defined as the beamforming vectors at the gNB and UE  $k$ , respectively. Let  $x_k$  be the single-stream signal transmitted by the gNB to UE  $k$ ; the received post-processing signal can be expressed as

$$z_k = \mathbf{v}_k^T \mathbf{G}_k \mathbf{\Phi} \mathbf{H} \mathbf{w}_k x_k + \mathbf{v}_k^T \mathbf{n}_k, \quad (2)$$

where  $\mathbf{n}_k \in \mathbb{C}^{N_U \times 1}$  represents the circularly symmetric complex Gaussian noise vector with entries having zero-mean and variance  $\sigma_n^2$ , while  $\mathbf{\Phi} \in \mathbb{C}^{N_I \times N_I}$  is the IRS configuration, i.e., a diagonal matrix defined as

$$\mathbf{\Phi} = \text{diag}(\phi_1, \dots, \phi_{N_I}). \quad (3)$$

Note that different, and specific, IRS configurations can be adopted for different UEs. Accordingly, in the rest of the paper we let  $\mathbf{\Phi}_k$  be the IRS configuration adopted when UE  $k$  is served.

The SNR at UE  $k$ , with IRS configuration  $\mathbf{\Phi}_k$ , is given by

$$\Gamma_k(\mathbf{\Phi}_k) = \frac{|\mathbf{v}_k^T \mathbf{G}_k \mathbf{\Phi}_k \mathbf{H} \mathbf{w}_k|^2 \sigma_x^2}{|\mathbf{v}_k|^2 \sigma_n^2}, \quad (4)$$

where  $\sigma_x^2$  is the power of the transmitted signal. To maximize the SNR of a given UE, a specific IRS configuration should be adopted, tailored to the UE position in the cell and the channel conditions. However, the goal of this paper is to limit the number of IRS reconfigurations to comply with realistic energy and overhead constraints, as well as to improve the communication efficiency, and algorithms seeking to comply with these requirements will be presented in Section III.

### B. Sum Capacity Optimization Problem

We impose a constraint on the number of IRS reconfigurations per time frame, with the goal of either limiting the reconfiguration overhead, or accounting for practical limitations that might arise in realistic deployments. On the downside, achieving this objective usually leads to SNR degradation as sub-optimal IRS configurations might be adopted for some UEs. To mitigate this effect, we formulate a constrained optimization problem on the average cell sum capacity. Specifically, we assume the following conditions:

1. at most  $Z$  IRS reconfigurations can occur per time frame;
2. the gNB serves  $K$  UEs by partitioning them into  $Z$  disjoint subsets  $\mathcal{U}_1, \dots, \mathcal{U}_Z$ ,  $Z \leq K$ ;
3. for each UE in  $\mathcal{U}_z$ , the same IRS configuration  $\mathbf{\Phi}^{(z)}$  is used, i.e.,  $\mathbf{\Phi}_k = \mathbf{\Phi}^{(z)}, \forall k \in \mathcal{U}_z, \forall 1 \leq z \leq Z$ .

Then, the achievable capacity/rate of UE  $k \in \mathcal{U}_z$  is

$$R_k(\mathbf{\Phi}^{(z)}) = \log_2 \left( 1 + \Gamma_k(\mathbf{\Phi}^{(z)}) \right), \quad (5)$$

where  $\Gamma_k(\mathbf{\Phi}^{(z)})$  is the SNR experienced by the  $k$ -th UE while configuration  $\mathbf{\Phi}^{(z)}$  is adopted at the IRS, i.e., the configuration shared by all UEs belonging to subset  $\mathcal{U}_z$ .

Let  $\mathcal{I} = \{\mathbf{\Phi}^{(1)}, \mathbf{\Phi}^{(2)}, \dots, \mathbf{\Phi}^{(Z)}\}$  be the set of IRS configurations corresponding to subsets  $\mathcal{U}_1, \dots, \mathcal{U}_Z$ . The system sum capacity within a time frame is defined as

$$C(\mathcal{U}_1, \dots, \mathcal{U}_Z, \mathcal{I}) = B \sum_{z=1}^Z \sum_{k \in \mathcal{U}_z} R_k(\mathbf{\Phi}^{(z)}), \quad (6)$$

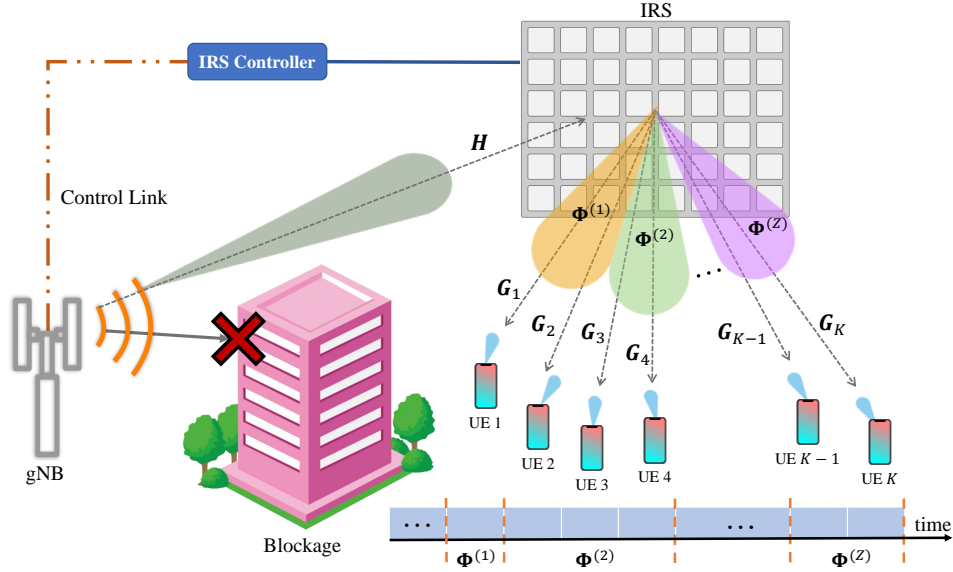


Fig. 1. Downlink TDMA scheduling for IRS-assisted multi-user communications.

where  $B$  is the transmission bandwidth. The optimization problem is then formulated as

$$\max_{\mathcal{U}_1, \dots, \mathcal{U}_Z, \mathcal{I}} C(\mathcal{U}_1, \dots, \mathcal{U}_Z, \mathcal{I}), \quad (7a)$$

$$\text{s.t.} \quad \angle[\Phi^{(z)}]_{n,n} \in \mathcal{P}_\theta, \quad n = 1, \dots, N_I, z = 1, \dots, Z. \quad (7b)$$

Problem (7) determines the optimal grouping strategy for the UEs subsets  $\mathcal{U}_1, \dots, \mathcal{U}_Z$ , and assigns the best IRS configuration accordingly. This can be viewed as a *clustering* problem, where the goal is to group, i.e., cluster, the UEs based on their channel characteristics. However, this is a mixed integer nonlinear programming (MINLP) problem, which is known to be NP-hard. As such, finding the optimal solutions may not be feasible, especially as  $N_I$  increases. Therefore, heuristic clustering algorithms can be used to obtain approximated, though close-to-optimal, solutions, as described in Section III.

### III. CONSTRAINED SUM CAPACITY OPTIMIZATION

In this section, we provide heuristic solutions to (7). First, we present two clustering-based approaches to identify and group UEs with a similar optimal IRS configuration. Then, we solve the scheduling problem on the identified clusters with a TDMA approach [37]. We compute the UEs clusters by first estimating the optimal individual IRS configurations, denoted as  $\Phi_k^*$ ,  $1 \leq k \leq K$ , i.e., the IRS configurations leading to the maximum capacity for each UE  $k$ , as described in Section III-A. These configurations would solve (7) for  $Z = K$ , as in this case all UEs are served in a TDMA fashion and with their optimal IRS configuration. The phase coefficients of the optimal IRS configuration matrices are then chosen as the initial points of a procedure leveraging arbitrary clustering algorithms in the  $N_I$ -dimensional space, as explained in Section III-B.

#### A. Optimal Individual IRS Configurations

In MIMO systems, both the gNB and the UEs adopt properly tuned beamformers to match the signal transmissions and receptions to the spatial direction providing the highest channel gain [11]. For the optimization of the IRS configuration of each individual UE, we adopt a procedure similar to that presented in [28], focusing on single-stream transmissions and, without loss of generality, on UE  $k$ .

The optimal beamforming vectors  $\mathbf{v}_k$  and  $\mathbf{w}_k$  coincide with the singular vectors corresponding to the highest singular value of the wireless channel matrix. In principle,  $\mathbf{v}_k$  and  $\mathbf{w}_k$  could be estimated by applying singular value decomposition (SVD) on the overall cascade channel matrix

$$\mathbf{G}_k \Phi_k \mathbf{H} = \mathbf{U} \Sigma \mathbf{V}^\dagger, \quad (8)$$

and obtaining the right and left singular vectors of  $\mathbf{G}_k \Phi_k \mathbf{H}$  as the columns of  $\mathbf{V}$  and  $\mathbf{U}$ , and the corresponding singular values as the diagonal entries of  $\Sigma$ . However, notice that the cascade channel itself depends on the specific IRS configuration  $\Phi_k$ , which in our formulation represents one of the optimization variables. Indeed, given  $\mathbf{v}_k$  and  $\mathbf{w}_k$ , we can solve

$$\Phi_k^* = \underset{\Phi_k}{\operatorname{argmax}} R_k(\Phi_k), \quad (9a)$$

$$\text{s.t.} \quad \angle[\Phi_k]_{n,n} \in \mathcal{P}_\theta, \quad n = 1, \dots, N_I. \quad (9b)$$

where  $R_k$  is the achievable capacity of UE  $k$ ,  $1 \leq k \leq K$ , according to (5). By defining  $\mathbf{s}_k = \mathbf{v}_k^\top \mathbf{G}$  and  $\mathbf{u}_k = \mathbf{H} \mathbf{w}_k$ , the signal power can be re-written as

$$|\mathbf{s}_k \Phi_k \mathbf{u}_k|^2 = \left| \sum_{n=1}^{N_I} |[\mathbf{s}_k]_n| |[\mathbf{u}_k]_n| e^{j(\angle[\mathbf{s}_k]_n + \theta_n + \angle[\mathbf{u}_k]_n)} \right|^2. \quad (10)$$

---

**Algorithm 1** Iterative Alternate IRS Optimization
 

---

**Require:**  $\mathbf{G}_k, \mathbf{H}$ 
**Ensure:**  $\Phi_k^*$ 

```

1:  $t \leftarrow 0$ 
2:  $\mathbf{v}_k, \mathbf{w}_k \leftarrow \mathbf{1}$ 
3: repeat
4:    $\mathbf{s}_k \leftarrow \mathbf{v}_k^T \mathbf{G}_k, \mathbf{u}_k \leftarrow \mathbf{H} \mathbf{w}_k$ 
5:    $\theta_{k,n} \leftarrow -(\angle[\mathbf{s}_k]_n + \angle[\mathbf{u}_k]_n)$ 
6:    $\angle[\Phi_{k,t}]_{n,n} \leftarrow \operatorname{argmin}_{\psi \in \mathcal{P}_\theta} (\angle e^{j(\theta_{k,n} - \psi)})$ 
7:    $\mathbf{U}, \Sigma, \mathbf{V}^\dagger \leftarrow \text{SVD of } \mathbf{v}_k^T \mathbf{G}_k \Phi_{k,t} \mathbf{H} \mathbf{w}_k$ 
8:    $\mathbf{v}_k \leftarrow$  column of  $\mathbf{V}$  corresponding to
     the largest singular value
9:    $\mathbf{w}_k \leftarrow$  column of  $\mathbf{U}$  corresponding to
     the largest singular value
10:   $t \leftarrow t + 1$ 
11: until  $|R_k(\Phi_{k,t}) - R_k(\Phi_{k,t-1})| < \epsilon$ 
12:  $\Phi_k^* \leftarrow \Phi_{k,t}$ 

```

---

Then, it is sufficient to observe that the SNR is maximized when the phase shifts introduced by the IRS are aligned with the phase shifts accumulated along the various paths, i.e.,

$$\theta_{k,n} = -(\angle[\mathbf{s}_k]_n + \angle[\mathbf{u}_k]_n), \quad \forall n. \quad (11)$$

Taking into account the possible quantization, the optimal phase shifts are given by

$$\angle[\Phi_k^*]_{n,n} \leftarrow \operatorname{argmin}_{\psi \in \mathcal{P}_\theta} (\angle e^{j(\theta_{k,n} - \psi)}), \quad \forall n. \quad (12)$$

To overcome the interdependence between optimal IRS configurations and beamforming vectors, we propose an iterative alternate optimization approach. We first estimate the optimal beamforming vectors for a given IRS configuration using (8). Then, we plug the derived beamformers into (9a), and obtain the corresponding optimal IRS configuration. We repeat this two-step procedure until convergence which, for practical purposes, is assumed to be reached when the difference between the achievable rates  $R_k, \forall k$ , in two consecutive iterations becomes lower than a tolerance  $\epsilon > 0$ . This procedure is summarized in Algorithm 1, where  $t$  is the iteration index. Notice that the number of required iterations grows with the number of antennas and of IRS phase shifters. However, from preliminary simulations, and based on the set of parameters we considered (see Section VI), convergence is typically reached in less than 10 iterations.

### B. Clustering-based TDMA Scheduling

For an approximated but close-to-optimal solution to (7), we resort to a clustering-based approach. Our proposed clustering algorithms estimate both the subsets of UEs  $\mathcal{U}_1, \dots, \mathcal{U}_Z$ , and the relative set of IRS configurations  $\mathcal{I}$ . We operate on the *phase vector space*, i.e., the points to be clustered are identified by the IRS phase shifts vector

$$[\angle\phi_1, \dots, \angle\phi_{N_1}]^T = [\theta_1, \dots, \theta_{N_1}]^T, \quad (13)$$

which maps each IRS configuration  $\Phi$  to a point in  $[-\pi, \pi]^{N_1}$ . Note that, in the case of quantized phase shifts, the actual

phase vector space is a discrete grid in the continuous space  $[-\pi, \pi]^{N_1}$ .

The general clustering-based procedure works as follows:

1. find  $\Phi_k^*, \forall k$ , i.e., the optimal individual IRS configurations for each UE as in Section III-A;
2. build UE subsets  $\mathcal{U}_z, z = 1, \dots, Z$ , by using an arbitrary clustering algorithm, according to the description in Sections IV and V;
3. assign  $\Phi^{(z)}$  to all UEs  $\in \mathcal{U}_z$ .

The core idea of this procedure, and the main contribution of this paper, is to use clustering algorithms to group users, and assign the respective IRS configurations, which are mapped to the *centroid* of the cluster. Notice that, in the case of quantized phase shifts, once the clustering procedure is performed, clusters may share the same centroid and be merged. Therefore,  $Z$  represents the *maximum number of clusters*, not the effective number. In the following, we propose different techniques to build the clusters based on either a distance metric (Section IV) or the actual achievable rate (Section V).

## IV. DISTANCE-BASED CLUSTERING ALGORITHMS

Distance-based clustering is a class of clustering methods that group data points based on their similarity or dissimilarity using a distance metric. This clustering approach has several advantages, including the efficiency in handling large datasets, and the flexibility to adapt to many different scenarios of interest. However, distance-based clustering can be sensitive to the choice of the distance metric (which depends on the nature of the data and the clustering problem), and the initialization of the algorithm. Moreover, in our specific case, it does not take into account the achievable rate, which is not directly related to the distance among the points in the phase vector space. We consider and compare some of the most popular distance-based clustering algorithms, namely, K-means, agglomerative hierarchical clustering, and K-medoids.

Since the scalar field is the range  $[-\pi, \pi)$ , the adopted distance has to take into account the circularity of data. Thus, we employ the *circular distance* metric, defined as

$$\delta(\boldsymbol{\alpha}, \boldsymbol{\beta}) = \sum_{n=1}^{N_1} \angle(e^{j(\angle[\boldsymbol{\alpha}]_n - \angle[\boldsymbol{\beta}]_n)}), \quad (14)$$

where  $\boldsymbol{\alpha}$  and  $\boldsymbol{\beta}$  are two generic complex vectors of length  $N_1$ .

*K-means (KM)*: K-means (KM) clustering [38] aims at finding  $Z$  disjoint clusters minimizing the within-cluster sum of squares. Here, we consider the well-known Lloyd algorithm [39], which randomly selects  $Z$  points in the space of phase vectors as the initial centroids. In our setup, in order to ensure optimal performance when  $Z = K$ , we force the algorithm initialization to a random selection among the phase vectors of the optimal individual IRS configurations derived in Section III-A. Then, KM assigns each data point to the closest centroid, according to the specified distance metric. The set of centroids is then re-computed as the average of all data points that belong to each cluster. These steps are repeated until either convergence or a maximum number of iterations  $J_{\max}^{\text{KM}}$  is reached.

*Agglomerative Hierarchical clustering (HC)*: The agglomerative hierarchical clustering (HC) [40] partitions a set of data points into disjoint clusters by iteratively merging points into clusters until a target number of partitions is met. In our setup, clusters are initialized as the optimal phase vectors, which thus act as the respective centroids. Then, the average distance between all pairs of data points in any two clusters is evaluated. The closest pair of clusters is merged into a new single cluster, whose centroid is computed as the average of all its data points. The procedure is repeated until the number of clusters is equal to  $Z$ .

*K-medoids (KMed)*: K-medoids (KMed) [41] is a clustering technique similar to KM, but instead of using the mean of the data points within each cluster, it uses the medoid, i.e., the data point that is closest to the center of the cluster. In our setup, the algorithm starts by randomly selecting  $Z$  medoids among the optimal phase vectors, then it iteratively assigns each data point to the closest medoid, and updates the medoid for each cluster as the data point that minimizes the sum of the distances to all other data points within the same cluster. The algorithm continues until the medoids no longer change.

## V. CAPACITY-BASED CLUSTERING ALGORITHMS

The distance-based clustering techniques presented in Section IV do not directly take into account the actual capacity achievable by the UEs, which is a crucial factor for the sum capacity maximization problem in (7). Thus, in the following subsections we propose original capacity-based clustering algorithms that go beyond the state of the art, namely CWC (Section V-A), OSCBC (Section V-B), and ICWC (Section V-C).

### A. Capacity-Weighted Clustering (CWC)

Similarly to distance-based clustering, also CWC proceeds iteratively. However, the stopping condition is based on the variation of the sum capacity of each cluster, rather than on the distance between the centroids. In this approach, the clustering algorithm itself weighs the users based on their achievable capacity, so that the parameters of the resulting clusters are closer to the ones preferred by the users with higher rates, thus promoting the maximization of the sum capacity.

Let  $\Phi_i^{(z)}$  be the IRS configuration of cluster  $\mathcal{U}_{z,i}$  at iteration  $i$ . UEs are initially sorted in decreasing order of achievable rate. The algorithm then selects the  $Z$  UEs providing the highest achievable capacity based on the expression in (5) with their optimal IRS configurations. Without loss of generality, we let  $z = 1, \dots, Z$  be the index of those UEs, and set  $\Phi_1^{(z)} = \Phi_z^*$ ,  $\forall 1 \leq z \leq Z$ , as the centroids of the initial clusters  $\mathcal{U}_{1,0}, \dots, \mathcal{U}_{Z,0}$ . In the following, for simplicity, we denote with  $z_{k,i}$  the cluster such that  $k \in \mathcal{U}_{z,i}$ . Each UE  $k > Z$  is assigned to the cluster whose centroid provides the lowest rate difference with respect to its ideal configuration, i.e.,

$$z_{k,i} = \underset{z}{\operatorname{argmin}} [R_k(\Phi_k^*) - R_k(\Phi_i^{(z)})]. \quad (15)$$

Note that, despite being always non-negative, the rate difference in (15) cannot be considered a distance metric as, in

---

### Algorithm 2 CWC Algorithm

---

**Require:**  $Z, \mathbf{H}, \mathbf{G}_k, \forall k$

**Ensure:**  $\mathcal{U}_1, \dots, \mathcal{U}_Z, \mathcal{I}$

- 1: Compute  $\Phi_k^*, \forall k$  with the procedure of Algorithm 1
  - 2:  $i \leftarrow 1$
  - 3: Sort the UEs in decreasing order of  $R_k(\Phi_k^*)$
  - 4: Select the  $Z$  UEs providing the highest  $R_k(\Phi_k^*)$ ,
  - 5: Set  $\Phi_1^{(z)} = \Phi_k^*, z = 1, \dots, Z$  as the initial centroids.
  - 6: **repeat**
  - 7:   **for** each UE  $k$  **do**
  - 8:      $z_{k,i} \leftarrow \operatorname{argmin}_z R_k(\Phi_k^*) - R_k(\Phi_i^{(z)})$
  - 9:   **end for**
  - 10:   **for** each cluster  $z$  **do**
  - 11:      $\Phi_{i+1}^{(z)} \leftarrow \frac{\sum_{k \in \mathcal{U}_z} \Phi_k^* R_k(\Phi_i^{(z)})}{\sum_{k \in \mathcal{U}_z} R_k(\Phi_i^{(z)})}$
  - 12:      $\angle[\Phi_{i+1}^{(z)}]_{n,n} \leftarrow \operatorname{argmin}_{\psi \in \mathcal{P}_\theta} \angle e^{j(\angle[\Phi_{i+1}^{(z)}]_{n,n} - \psi)}, \forall n$
  - 13:   **end for**
  - 14:    $i \leftarrow i + 1$
  - 15: **until**  $\left| \sum_{k \in \mathcal{U}_z} R_k(\Phi_i^{(z)}) - \sum_{k \in \mathcal{U}_z} R_k(\Phi_{i-1}^{(z)}) \right| < \mu$
  - 16: Assign  $\Phi^{(z)}$  to all  $k \in \mathcal{U}_z$ .
- 

general, it does not satisfy the triangle inequality. After all the remaining UEs have been assigned to the corresponding clusters, the coordinates of the centroids need to be updated. At iteration  $i + 1$ , the new IRS configuration of cluster  $\mathcal{U}_{z,i+1}$  is computed as the average of all data points in the cluster, weighted by their achievable rate, i.e.,

$$\Phi_{i+1}^{(z)} = \frac{\sum_{k \in \mathcal{U}_z} \Phi_k^* R_k(\Phi_i^{(z)})}{\sum_{k \in \mathcal{U}_z} R_k(\Phi_i^{(z)})}. \quad (16)$$

Then, in the case of phase shifter quantization, the additional approximation step must be performed as

$$\angle[\Phi_{i+1}^{(z)}]_{n,n} \leftarrow \operatorname{argmin}_{\psi \in \mathcal{P}_\theta} \left( \angle e^{j(\angle[\Phi_{i+1}^{(z)}]_{n,n} - \psi)} \right), \quad \forall n. \quad (17)$$

This two-step procedure is repeated until convergence, which is reached when the rate difference between two consecutive iterations is lower than the sum capacity tolerance  $\mu > 0$ .

The rationale behind the algorithm is that, based on the initial centroid assignment, the UEs experiencing the best channel conditions, i.e., those dominating the system sum capacity, are initially served with their optimal (individual) IRS configurations. Even after the adjustment of the clusters, these UEs will always get the largest weight coefficient within the cluster. The remaining UEs, instead, will be penalized by the configuration constraints, but their impact on the sum capacity will be limited. The whole workflow of the CWC procedure is summarized in Algorithm 2.

### B. One-Shot Capacity-Based Clustering (OSCBC)

The main drawback of CWC presented in Section V-A is that it requires solving problem (15) at each iteration, relative to all the UEs in each cluster. Considering massive MIMO systems, the CWC procedure could become exceedingly complex, as it requires the SVD computation of extremely large

matrices. Therefore, we propose another lower-complexity clustering algorithm, denoted as OSCBC.

As in CWC, also in OSCBC: (i) the UEs are sorted in decreasing order of achievable rate; (ii) the  $Z$  IRS configurations of the  $Z$  UEs experiencing the highest rates are chosen as initial centroids for the clusters; and (iii) the remaining UEs are assigned to the closest centroid in terms of circular distance, as per (14). Then, compared to CWC, instead of recomputing the coordinates of the centroids at each iteration until convergence, the algorithm stops right after the initial association. Therefore, with OSCBC the computed centroids are the optimal configurations relative to the  $Z$  UEs achieving the highest individual rate, which provides sub-optimal (non-optimized) performance for the rest of the UEs in the clusters.

### C. Inverse Capacity-Weighted Clustering (ICWC)

The CWC algorithm is designed to optimize the capacity of the UEs experiencing the best channel conditions only, and is unfair with respect to the other UEs in the system which may use sub-optimal IRS configurations. Therefore, we propose an additional variation of CWC, named ICWC, with the goal of achieving higher fairness among the UEs in the system. In ICWC, while the cluster association principle expressed in (15) is preserved, the initial condition is reversed. Specifically: (i) UEs are sorted in increasing order of achievable rate; (ii) the initial configurations of the clusters  $\Phi_1^{(z)} = \Phi_z^*$ ,  $z = 1, \dots, Z$ , are based on the optimal configurations of the UEs with the worst channel conditions. The remaining  $k > Z$  UEs are then associated as in (15). Then, at iteration  $i$ , the IRS configuration is updated as

$$\Phi_{i+1}^{(z)} = \frac{\sum_{k \in \mathcal{U}_z} \Phi_k^* R_k^{-1}(\Phi_i^{(z)})}{\sum_{k \in \mathcal{U}_z} R_k^{-1}(\Phi_i^{(z)})}, \quad (18)$$

and the discretization step (17) is performed (if needed). As in CWC, convergence is achieved if the rate difference between two consecutive iterations is lower than the tolerance  $\mu$ . While ICWC is sub-optimal, in terms of sum capacity, with respect to CWC, it can provide significant improvements in terms of fairness, especially from the perspective of the users with the worst channel conditions.

## VI. NUMERICAL RESULTS

In this section, we present our simulation parameters (Section VI-A) and metrics (Section VI-B), and assess via simulation the complexity (Section VI-C) and scheduling (Section VI-D) performance of an IRS-assisted network with practical constraints in various scenarios.

### A. Simulation Parameters

Our simulation parameters are reported in Table I.

*Scenario.* All devices are assumed to lie on a 2D plane, and we consider an urban micro-cell (UMi) scenario, according to the 3GPP nomenclature [42], with the gNB placed at the center. According to the 3GPP specifications, the coverage area of the gNB is characterized by an average radius of 167 m and is assumed to lie in the positive  $x$ -axis region.

TABLE I  
SIMULATION PARAMETERS.

Parameter	Value
Carrier frequency	28 GHz
Total bandwidth ( $B$ )	100 MHz
Noise spectral density	-174 dBm/Hz
Number of UEs ( $K$ )	100
gNB antenna array ( $N_g$ )	8H×8V
gNB transmit power	33 dBm
UE antenna array ( $N_U$ )	2H×1V
IRS elements ( $N_I$ )	{10H×20V, 20H×40V, 40H×80V, 60H×120V}
Phase shift quant. bits ( $b$ )	{unquantized, 1-bit, 2-bits}
LoS probability ( $p_{\text{LoS}}$ )	Eq. (20)
Individual rate opt. tolerance ( $\epsilon$ )	$10^{-6}$ [bit/s/Hz]
KM max. iterations ( $I_{\text{max}}^{\text{KM}}$ )	50
CWC/ICWC rate tolerance ( $\mu$ )	$10^{-3}$ [bit/s]

We assume that  $K = 100$  UEs are randomly deployed according to a uniform distribution within the cell area, to be served in downlink by the gNB, assisted by an IRS at coordinates (75, 100) m. The gNB is equipped with a uniform planar array (UPA) with 8H×8V antennas (i.e.,  $N_g = 64$ ), and the UEs with uniform linear arrays (ULAs) of 2H×1V antennas (i.e.,  $N_U = 2$ ). For the IRS, if not otherwise specified, we adopt a 40H×80V reflective panel ( $N_I = 3200$ ).

*Channel.* The system operates at a carrier frequency of 28 GHz (that is in the lower part of the mmWave bands), the transmission power at the gNB is set to 33 dBm, and the noise power spectral density at the receivers is -174 dBm/Hz. Finally, the total system bandwidth is 100 MHz. We consider the 3GPP TR 38.901 spatial channel model [42], which supports a wide range of frequencies, from 0.5 to 100 GHz (and including therefore our carrier frequency of 28 GHz), and can be integrated with realistic beamforming models. As such, channel matrices, and multipath fading, are computed based on the superposition of  $N$  different clusters, each of which consists of  $M$  rays that arrive (depart) to (from) the antenna arrays with specific angles and powers. Based on [42], and using the simplifications proposed in [43], the generic entry  $[\mathbf{A}]_{pq}$  of the channel matrix can then be computed as:

$$[\mathbf{A}]_{pq} = \gamma \sum_{n=1}^N \sqrt{\frac{P_n}{M}} \sum_{m=1}^M \bar{\mathbf{F}}_{rx}(\theta_{n,m}^A, \phi_{n,m}^A) \times \begin{bmatrix} e^{j\Phi_{n,m}^{\theta}} & \sqrt{K_{n,m}^{-1}} e^{j\Phi_{n,m}^{\theta}} \\ \sqrt{K_{n,m}^{-1}} e^{j\Phi_{n,m}^{\theta}} & e^{j\Phi_{n,m}^{\phi}} \end{bmatrix} \times \bar{\mathbf{F}}_{tx}(\theta_{n,m}^D, \phi_{n,m}^D) \times e^{j\bar{\mathbf{k}}_{rx,n,m}^T \bar{\mathbf{a}}_{rx,p} e^{j\bar{\mathbf{k}}_{tx,n,m}^T \bar{\mathbf{a}}_{tx,q}}, \quad (19)$$

where  $\gamma$  is the large-scale fading coefficient (LSFC) of the considered link, which incorporates the path loss and shadowing terms.<sup>1</sup> Specifically, while the gNB and the IRS can be assumed to operate in line-of-sight (LoS), the path loss

<sup>1</sup>For a complete description of the remaining terms appearing in (19) we refer the interested reader to [43].

between a generic UE  $k$  and the IRS is modeled based on the following channel conditions:

- *non-line-of-sight (NLoS)*: UE  $k$  is in NLoS with the IRS;
- *deterministic LoS (LoS)*: UE  $k$  is in LoS with the IRS;
- *probabilistic LoS (LoS)*: the IRS-UE  $k$  link can be in LoS with probability

$$p_k^{\text{LoS}}(d_k) = \begin{cases} 1 & \text{if } d_k \leq 18, \\ \frac{18}{d_k} + \left(1 - \frac{18}{d_k}\right) e^{-\frac{d_k}{36}} & \text{if } d_k > 18, \end{cases} \quad (20)$$

where  $d_k$  is the distance (in meters) between the IRS and UE  $k$ , while it is in NLoS with probability  $1 - p_k^{\text{LoS}}(d_k)$ . In the considered UMi scenario, and based on the 3GPP specifications [42], the average LoS probability in (20) is 0.35.

For each wireless link, based on the presence of the LoS component, the path loss is then derived according to [42, Table 7.4.1-1], with shadowing standard deviation set to  $\sigma_{\text{SF}} = 0$ .

For the optimal individual IRS configuration (Section III-A), we set  $\epsilon = 10^{-6}$  [bit/s/Hz].

*Clustering algorithms.* In the following subsections we present extensive simulation results to compare the performance of distance-based (KM, HC, KMed) vs. capacity-based (CWC, OSCBC, ICWC) clustering algorithms to perform scheduling in an IRS system with reconfiguration constraints. The KM clustering has been implemented with the Lloyd algorithm [39] with a maximum number of  $I_{\text{max}}^{\text{KM}} = 50$  iterations, while, for KMed, we use the partition around medoids (PAM) method [44]. For managing the circularity of the phase shifts, we used some tools from [45]. Instead, for both CWC and ICWC, we set  $\mu = 10^{-3}$  [bit/s].

As an upper bound to the system performance, we also consider an “unclustered” scheduling, wherein we assume that all UEs are served with their optimal IRS configuration. This scheduling clearly violates the constraint on the maximum numbers of reconfiguration per frame, but can be regarded as the limit case when  $Z = K$ , i.e., all UEs belong to a cluster with cardinality one. As such, it is a suitable approach for benchmarking the performance of more practical schemes.

## B. Performance Metrics

The performance of the proposed clustering-based scheduling techniques is evaluated in terms of computational complexity, average sum capacity, and fairness, as a function of different channel conditions, IRS dimensions, and degrees of quantization for the phase shifts.

*Computational complexity.* It is computed as the number of iterations that each of the clustering algorithms require to: (i) obtain the optimal IRS configuration of each UE; (ii) partition the UEs into disjoint subsets, or clusters, based on distance or capacity metrics; and (iii) for each cluster, find the best IRS configuration to serve the corresponding UEs.

*Average sum capacity.* It is derived from (6) as

$$\bar{C} = \frac{1}{K} \mathbb{E}[C(\mathcal{U}_1, \dots, \mathcal{U}_Z, \mathcal{I})], \quad (21)$$

TABLE II  
COMPUTATIONAL COMPLEXITY OF DISTANCE-BASED VS. CAPACITY-BASED CLUSTERING.

Clustering algorithm	Computational complexity
KM (Lloyd)	$O(IZK)$
KMed (PAM)	$O(Z^3 K^2)$
HC	$O(K^3)$
CWC/ICWC	$O(IZKN_g N_U \min(N_g, N_U))$
OSCBC	$O(Z(K - Z))$

where the expectation is computed across the different channel realizations. Moreover, we average over the time slots, dividing the empirical expectation by the number of users (slots)  $K$ .

*Fairness.* We consider the 95% percentile of the achieved individual rate, computed as

$$C_{95\%} = \frac{B}{K} \inf\{x : \text{CDF}(x) \geq 0.95\}, \quad (22)$$

where  $\text{CDF}(\cdot)$  is the empirical cumulative distribution function of  $R_k(\Phi^{(z)})$ ,  $\forall k, z$ , and  $\inf$  denotes the infimum of the set of values of  $x$  that satisfy the inequality.

## C. Computational Complexity

In Table II we compare the computational complexity of the clustering algorithms presented in Sections IV and V. In all the algorithms, the first step is to obtain the optimal IRS configuration of each UE, as described in Section III-A. At each iteration, the main source of complexity is the SVD computation of the overall cascade channel matrix  $\mathbf{G}_k \Phi_k \mathbf{H}$ , which has complexity  $O(N_g N_U \min(N_g, N_U))$  [46]. Additionally, in case of quantized IRS phase shifts, after obtaining the optimal beamformers, the optimal phase shifts for the IRS are obtained through exhaustive search over the set of possible phase shifts  $\mathcal{P}_\theta$ , yielding a complexity of  $O(2^b N_I)$ .

Notice that different clustering algorithms may need a different number of iterations to reach convergence, which has some practical limitations. In the following,  $I$  denotes the number of iterations, assumed for simplicity to be the same for all the clustering strategies.

*Distance-based clustering.* These algorithms do not require specific initialization. For KM, based on the Lloyd implementation in [39], each iteration involves calculating the distances between data points and centroids. As a result, the computational complexity is influenced by the number of iterations required for convergence, the number of data points, the number of clusters, and the dimensionality of data, resulting in an overall complexity of  $O(IZK)$ . For KMed, implemented with the PAM algorithm, the total computational complexity is  $O(Z^3 K^2)$ , due to the pairwise distance computations between data points and medoids. Finally, the computational complexity of the agglomerate HC is primarily determined by the computation of pairwise distances among all data points, resulting in a total complexity of  $O(K^3)$  [47].



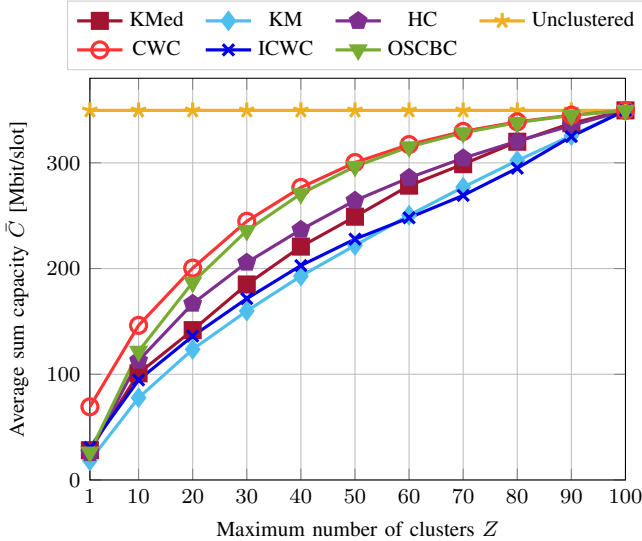


Fig. 2. Average sum capacity as a function of the maximum number of clusters  $Z$ , for an unquantized  $40\text{H}\times 80\text{V}$  IRS, and considering a pLoS channel for the IRS-UEs links.

*Capacity-based clustering.* Notably, capacity-based clustering needs an initialization stage wherein the algorithms select the  $Z$  UEs providing the highest (or lowest)  $R_k(\Phi_k^*)$ , which requires sorting the  $K$  rates obtained for the  $K$  UEs using their optimal IRS configuration, and selecting the top  $Z$ , resulting in a complexity of  $O(K \log K)$ . In the following iterations, both CWC and ICWC compute the rate difference between each UE and the  $Z$  centroids. The complexity of computing  $R_k(\Phi_i^{(z)})$  is dominated by the complexity of the SVD performed at each iteration, for each UE and each current centroid, which requires  $O(IZKN_g N_U \min(N_g, N_U))$  operations. Then, the computation of the centroids as per (16)-(18) requires  $O(K)$  iterations. Finally, the complexity of the OSCBC algorithm is dominated by the centroid assignment upon initialization, and goes as  $O(Z(K - Z))$ .

#### D. Scheduling Performance

In this section we compare the IRS scheduling performance considering distance-based vs. capacity-based clustering, and as a function of different channel conditions, reconfiguration constraints, and degrees of quantization of the phase shifts.

*Impact of the clustering algorithm.* First, Fig. 2 displays the average sum capacity  $\bar{C}$  per slot as a function of the number of clusters  $Z$ , for unquantized IRS phase shifts, and considering a pLoS channel for the IRS-UEs links. It is evident that all the scheduling policies perform better whenever  $Z$  increases, and converge to the “unclustered” policy when  $Z = K$ . In fact, increasing the number of clusters corresponds to a smaller intra-cluster average distance, which eventually becomes zero when  $Z = K$ . Among the considered clustering policies, CWC and OSCBC provide the highest sum capacity, as they are designed to maximize  $\bar{C}$ , and choose the IRS configurations of the UEs that achieve the highest rate. Instead, distance-based clustering achieves lower performance as it does not exploit the knowledge of the rate achievable with different IRS

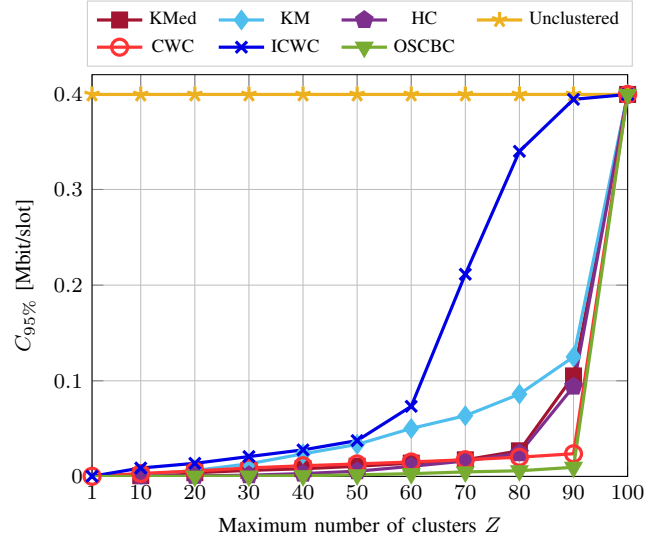


Fig. 3. 95% percentile of the average sum capacity as a function of the maximum number of clusters  $Z$ , for an unquantized  $40\text{H}\times 80\text{V}$  IRS, and considering a pLoS channel for the IRS-UEs links.

configurations when building the clusters. As expected, ICWC is designed to promote fairness, thus underperforms both CWC and OSCBC in terms of sum capacity; still, it achieves similar performance as distance-based clustering. Finally, the gap between CWC and OSCBC is almost negligible: this implies that a single iteration in the clustering process is enough to achieve good sum capacity, while also promoting lower computational complexity as reported in Table II, which demonstrates the good scalability of the proposed techniques.

Fig. 3 compares the fairness performance of the different clustering algorithms, measured as the 95% percentile of the average sum capacity  $C_{95\%}$ , as a function of the maximum number of clusters  $Z$  in pLoS conditions. Our results identify ICWC as the best clustering approach in terms of fairness, which comes at the cost of a lower sum capacity, as shown in Fig. 2. Therefore, there exists a trade-off between the achievable sum capacity and fairness. We also observe that OSCBC achieves very low fairness, as the UEs with worst channel conditions are forced to aggregate to the strongest UEs, thus via a sub-optimal IRS configuration. On the other hand, we see that CWC is more than acceptable in terms of fairness, and achieves comparable performance than most of the distance-based clustering algorithms. Finally, notice that  $C_{95\%}$  increases as  $Z$  increases, and eventually approaches the “unclustered” baseline for  $Z = K$ . This is due to the fact that the LoS probability in the pLoS scenario increases with the number of clusters, i.e., as the inter-cluster distance becomes smaller, which permits to experience better channel conditions, thus a higher capacity, even for the worst UEs.

*Impact of the channel.* From the above results, we concluded that distance-based clustering provides lower sum capacity and fairness compared to capacity-based scheduling, so the rest of our simulation campaign has been focused on the latter. Figs. 4 and 5 display the average sum capacity and the 95% percentile, respectively, for CWC, ICWC, and OSCBC

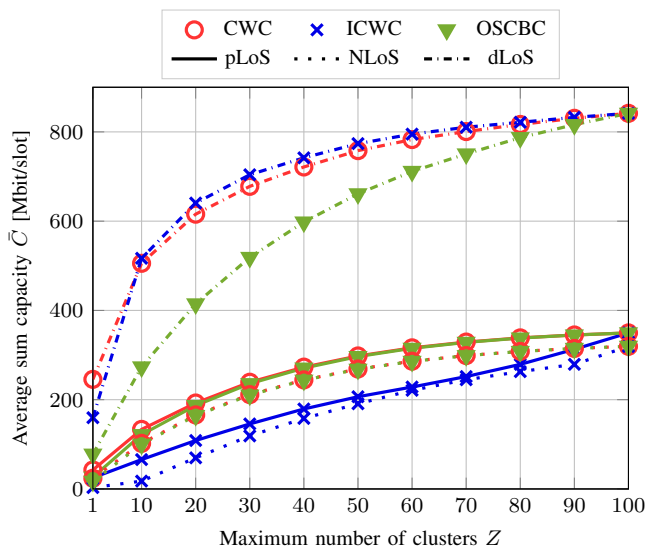


Fig. 4. Average sum capacity as a function of the maximum number of clusters  $Z$ , for  $N_I = 3200$ , unquantized phase shifts, and for different channel conditions.

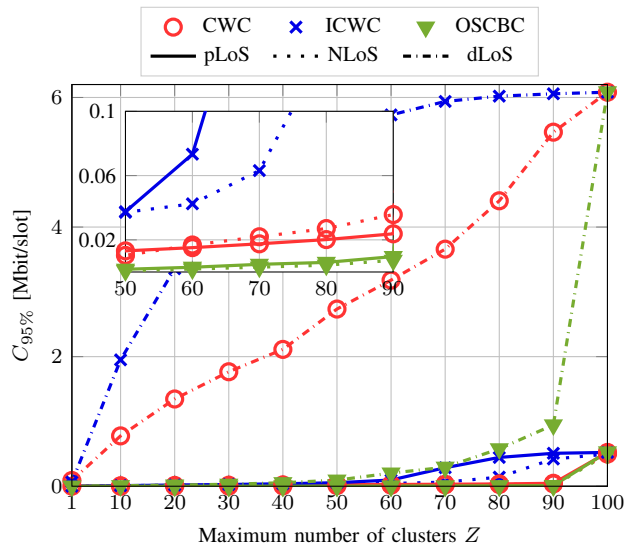


Fig. 5. 95% of the average sum capacity as a function of the maximum number of clusters  $Z$ , for  $N_I = 3200$ , unquantized phase shifts, and for different channel conditions. The zoom inside the figure is for  $50 \leq Z \leq 90$ .

in different channel conditions. First, we observe that in the dLoS scenario, where UEs are in LoS with the IRS, the sum capacity is up to 3.5 (2.5) times higher than in the NLoS (pLoS) scenario. This is mainly due to the fact that NLoS links experience (i) a higher path loss, and (ii) the lack of a dominant multipath component, thus of a clear steering direction for the IRS beam, which deteriorates the link quality. In particular, in the pLoS scenario the LoS probability decreases exponentially with the distance, therefore, the UEs that are far from the IRS typically operate in NLoS. For similar reasons, both CWC and ICWC in the dLoS scenario start to reach stability in terms of capacity with a relatively lower number of clusters than in the pLoS and NLoS scenarios.

As expected, OSCBC performs worse than its competitors,

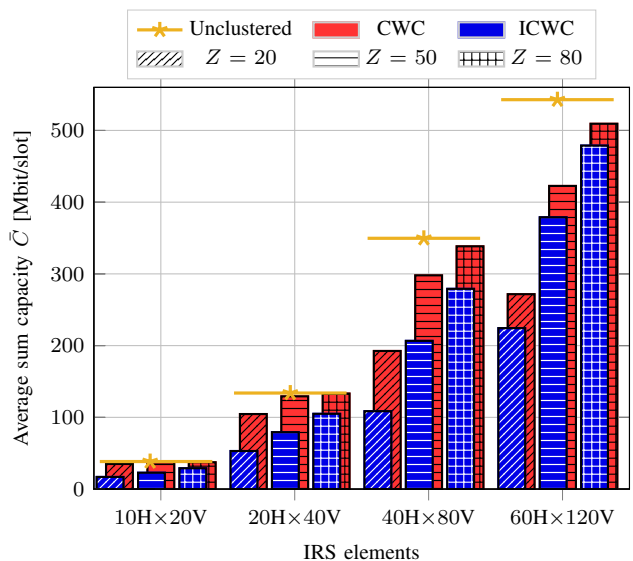


Fig. 6. Average sum capacity for CWC and ICWC as a function of the number of reflecting elements at the IRS, for unquantized phase shifts, and considering a pLoS channel for the IRS-UEs links.

and the gap is even more significant in the dLoS scenario (around  $-30\%$  in terms of sum capacity). The bad performance of OSCBC compared to CWC and ICWC is confirmed also in terms of fairness, as illustrated in Fig. 5 (see, in particular, the zoom for  $50 \leq Z \leq 90$ ).

Finally, even though ICWC is not explicitly designed to maximize the sum capacity, it shows similar performance (if not even slightly better) as CWC in the dLoS scenario. The rationale behind this behavior is not clear and deserves more investigation. Most likely, it is related to the fact that, in the dLoS scenario, all UEs have similar channel conditions, which permits ICWC to choose, on average, a good IRS configuration even among the worst UEs in the clusters.

*Impact of the IRS configuration.* Figs. 6 and 7 show the impact of the number of IRS radiating elements on the system performance when considering the CWC and ICWC clustering algorithms. As expected, both fairness (measured in terms of the 95% percentile of the average sum capacity) and sum capacity increase as the IRS is larger and operates with more reflecting elements, regardless of the number of clusters. For example, we observe that CWC is able to approach the optimal sum capacity with as few as 20 clusters for small-sized IRS, i.e., with  $10H \times 20V$  or  $20H \times 40V$  arrays. The same trends are shown also in Fig. 7 also in terms of fairness. Still, notice that  $\bar{C}$  is below 100 Mbps, which is not compatible with the requirement of most 5G applications when the IRS is made of fewer than 200 elements, which justifies the use of larger IRS panels [16].

Nevertheless, we still observe that the number of reflecting elements has an impact on the number of clusters that are needed to provide maximum performance. Indeed, the number of possible IRS configurations increases as we consider larger IRS antennas. In turn, this decreases the likelihood of UEs having the same (or similar) ideal configurations, and therefore, it increases the probability of being associated with

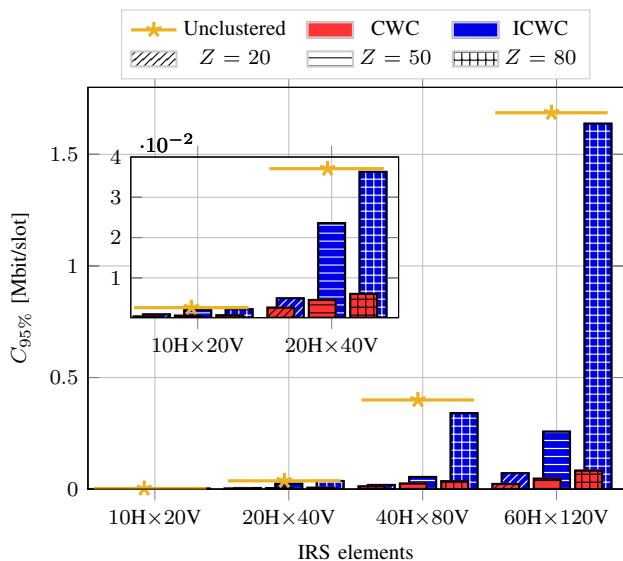


Fig. 7. 95% percentile of the average sum capacity for CWC and ICWC as a function of the number of reflecting elements at the IRS, for unquantized phase shifts, and considering a pLoS channel for the IRS-UEs links. The zoom inside the figure is for an IRS size of  $10\text{H}\times 20\text{V}$  ( $N_I = 200$ ) and  $20\text{H}\times 40\text{V}$  ( $N_I = 800$ ).

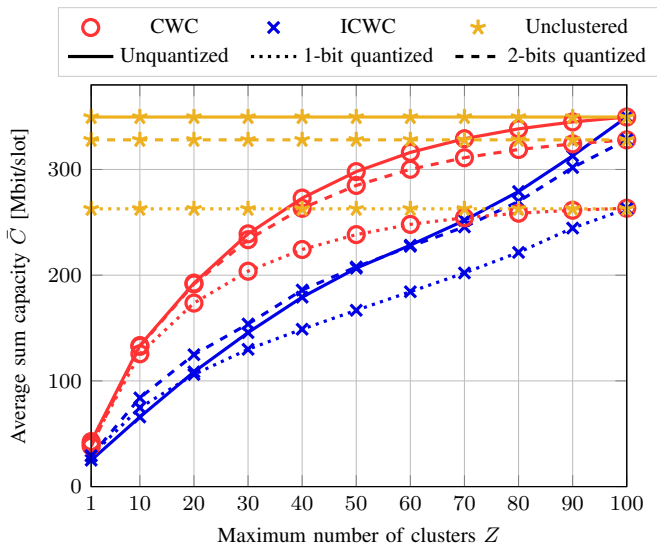


Fig. 8. Average sum capacity as a function of the maximum number of clusters  $Z$ , for  $N_I = 3200$  and for different degrees of quantization of the phase shifts, and considering a pLoS channel for the IRS-UEs links.

increasingly sub-optimal centroids if the number of clusters is small. However, if the number of phase shifters is large, the sub-optimality is mitigated by the increasing number of reconfigurations.

*Impact of quantization.* Figs. 8 and 9 display the average sum capacity and the 95% percentile, respectively, as a function of the maximum number of clusters  $Z$  for CWC and ICWC, and of the number of quantization bits  $b$  of the phase shifts. Notice that energy and hardware constraints pose a limit to  $b$  [48], which implies restricting the infinite set of possible IRS configurations to a finite set of cardinality  $2^{bN_I}$ . Moreover, the quantization constraint affects the beamforming

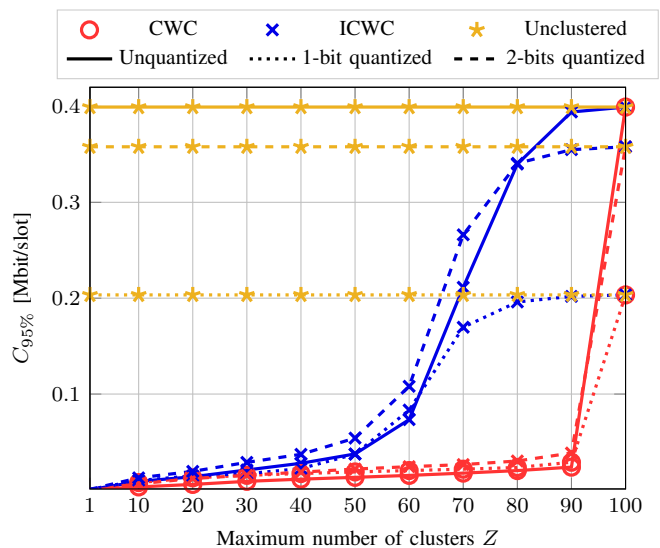


Fig. 9. 95% of the average sum capacity as a function of the maximum number of clusters  $Z$ , for  $N_I = 3200$  and for different degrees of quantization of the phase shifts, and considering a pLoS channel for the IRS-UEs links.

capabilities of the IRS [14], with negative implications for the resulting achievable sum capacity. In [1], results were obtained considering that the quantization was performed only at the end of the clustering procedure. Here, instead, we assume that the quantization of the phase shifts is taken into account from the initial optimization stage. The results reveal that the use of non-ideal phase shifters leads to a 30% degradation in the sum capacity when using  $b = 1$  at the IRS, while the performance is close to the unquantized baseline if more quantization bits are used. Furthermore, it is shown that the gap between quantized the unquantized performance increases with  $Z$ . As a result, 1-bit quantization is sufficient to guarantee performance comparable to the unquantized case with a low number of clusters, while more quantization bits are needed to achieve higher capacity. In any case, we can conclude that our proposed capacity-based clustering algorithms are robust to phase-shift quantization.

*Scalability.* Finally, we prove the scalability performance of the proposed clustering algorithms. To do so, Fig. 10 depicts the average minimum number of IRS configurations  $Z_{\min}$  needed to achieve 80% of the maximum achievable sum capacity (“unclustered” baseline) as a function of the number of UEs  $K$  in the system. Notably, we observe that CWC and OSCBC are confirmed to be the best algorithms to optimize the sum capacity, even for a limited number of IRS configurations. For example, both solutions achieve 80% of the maximum sum capacity with less than half the number of configurations than in the “unclustered” deployment. Moreover, we recognize the same trends as in the previous results. Specifically, capacity-based clustering outperforms distance-based clustering and requires fewer IRS reconfigurations to maximize the sum capacity (up to  $-37\%$  considering CWC vs. KMed). Furthermore, the gap increases as the number of UEs increases.

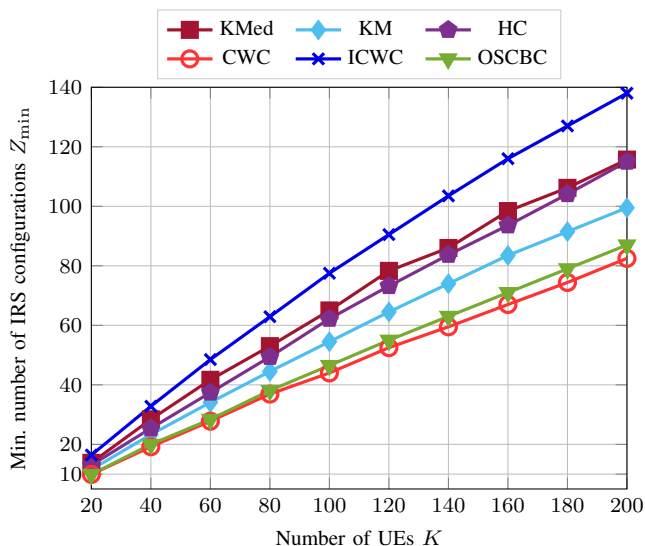


Fig. 10. Minimum number of IRS configurations (clusters)  $Z_{\min}$  to achieve 80% of the maximum achievable sum capacity, for an unquantized 40H $\times$ 80V IRS, and considering a pLoS channel for the IRS-UEs links.

## VII. CONCLUSIONS

In this paper we considered a MIMO cellular network in which a gNB serving multiple UEs encounters deep blockage, and is thus assisted by an IRS acting as a relay. Specifically, we considered practical constraints on the IRS reconfiguration period. We studied a TDMA scheduling for downlink transmissions, and formulated an optimization problem to maximize the average sum capacity, subject to a fixed number of IRS reconfigurations per time frame.

At first, we discussed an iterative algorithm to obtain the optimal IRS configuration of each UE. The performance degradation caused by the constraint in the number of possible reconfigurations was mitigated by proposing clustering-based scheduling policies, which group UEs with similar (ideal) IRS configurations based on either a distance metric or the achievable rate. This reduces the number of reconfigurations since all the UEs belonging to the same group/cluster are served with the same IRS parameters.

The performance of the different clustering algorithms was evaluated via simulations in terms of computational complexity, sum capacity, and fairness in different channel conditions for the IRS-UEs links, and as a function of the IRS size and quantization of phase shifts. The results showed that capacity-based clustering outperforms distance-based clustering, and can achieve up to 85% of the sum capacity obtained in an ideal deployment (with no reconfiguration constraints). Furthermore, we can reduce by 50% the number of IRS reconfigurations, thus reducing the reconfiguration overhead and promoting communication efficiency. Furthermore, we observed that ICWC, which was designed to promote fairness during scheduling, could also provide good performance in terms of capacity, especially to the UEs in poor channel conditions.

## REFERENCES

- [1] A. Rech, M. Pagin, S. Tomasin, F. Moretto, L. Badia, M. Giordani, J. Gambini, and M. Zorzi, "Downlink TDMA scheduling for IRS-aided communications with block-static constraints," in *Proc. IEEE WCNC WKSHPs*, 2023.
- [2] 3GPP, "NR; Base Station (BS) radio transmission and reception," TS 38.104 (Rel. 17), 2022.
- [3] F. Tariq, M. R. Khandaker, K.-K. Wong, M. A. Imran, M. Bennis, and M. Debbah, "A speculative study on 6G," *IEEE Wireless Commun.*, vol. 27, no. 4, pp. 118–125, Aug. 2020.
- [4] S. Rangan, T. S. Rappaport, and E. Erkip, "Millimeter-wave cellular wireless networks: Potentials and challenges," *Proc. IEEE*, vol. 102, no. 3, pp. 366–385, Mar. 2014.
- [5] P. Di Francesco, J. Kibitda, F. Malandrino, N. J. Kaminski, and L. A. DaSilva, "Sensitivity analysis on service-driven network planning," *IEEE/ACM Transactions on Networking*, vol. 25, no. 3, pp. 1417–1430, Jun. 2017.
- [6] E. J. Oughton, N. Comini, V. Foster, and J. W. Hall, "Policy choices can help keep 4G and 5G universal broadband affordable," *Techn. Forecasting Soc. Change*, vol. 176, p. 121409, 2022.
- [7] A. Chaoub, M. Giordani, B. Lall, V. Bhatia, A. Kliks, L. Mendes, K. Rabie, H. Saarnisaari, A. Singhal, N. Zhang *et al.*, "6G for bridging the digital divide: Wireless connectivity to remote areas," *IEEE Wireless Commun.*, vol. 29, no. 1, pp. 160–168, Feb. 2021.
- [8] D. López-Pérez, M. Ding, H. Claussen, and A. H. Jafari, "Towards 1 Gbps/UE in cellular systems: Understanding ultra-dense small cell deployments," *IEEE Commun. Surveys Tuts.*, vol. 17, no. 4, pp. 2078–2101, Oct.–Dec. 2015.
- [9] 3GPP, "NR; Study on integrated access and backhaul; Release 15," TR 38.874, 2018.
- [10] M. Polese, M. Giordani, T. Zugno, A. Roy, S. Goyal, D. Castor, and M. Zorzi, "Integrated access and backhaul in 5G mmWave networks: Potential and challenges," *IEEE Commun. Mag.*, vol. 58, no. 3, pp. 62–68, Mar. 2020.
- [11] R. Flamini, D. De Donno, J. Gambini, F. Giuppi, C. Mazzucco, A. Milani, and L. Resteghini, "Towards a heterogeneous smart electromagnetic environment for millimeter-wave communications: An industrial viewpoint," *IEEE Trans. Antennas Propag.*, vol. 70, no. 10, pp. 8898–8910, Oct. 2022.
- [12] E. Björnson, Ö. Özdogan, and E. G. Larsson, "Intelligent reflecting surface versus decode-and-forward: How large surfaces are needed to beat relaying?" *IEEE Commun. Lett.*, vol. 9, no. 2, pp. 244–248, Feb. 2020.
- [13] Q. Wu and R. Zhang, "Towards smart and reconfigurable environment: Intelligent reflecting surface aided wireless network," *IEEE Commun. Mag.*, vol. 58, no. 1, pp. 106–112, Jan. 2020.
- [14] S. Abeywickrama, R. Zhang, Q. Wu, and C. Yuen, "Intelligent reflecting surface: Practical phase shift model and beamforming optimization," *IEEE Trans. Commun.*, vol. 68, no. 9, pp. 5849–5863, Sep. 2020.
- [15] Q. Wu and R. Zhang, "Intelligent reflecting surface enhanced wireless network via joint active and passive beamforming," *IEEE Trans. Wireless Commun.*, vol. 18, no. 11, pp. 5394–5409, Nov. 2019.
- [16] M. Pagin, M. Giordani, A. A. Gargari, A. Rech, F. Moretto, S. Tomasin, J. Gambini, and M. Zorzi, "End-to-end simulation of 5G networks assisted by IRS and AF relays," in *Proc. IEEE MedComNet*, 2022.
- [17] R. Liu, Q. Wu, M. Di Renzo, and Y. Yuan, "A path to smart radio environments: An industrial viewpoint on reconfigurable intelligent surfaces," *IEEE Wireless Commun.*, vol. 29, no. 1, pp. 202–208, Jan. 2022.
- [18] C. Liaskos, S. Nie, A. Tsioliariidou, A. Pitsillides, S. Ioannidis, and I. Akyildiz, "Realizing wireless communication through software-defined hypersurface environments," in *Proc. IEEE WoWMoM*, 2018.
- [19] Y. Yang, S. Zhang, and R. Zhang, "IRS-enhanced OFDMA: Joint resource allocation and passive beamforming optimization," *IEEE Wireless Commun. Lett.*, vol. 9, no. 6, pp. 760–764, Jun. 2020.
- [20] J. Lee, J. Choi, and J. Kang, "Harmony search-based optimization for multi-RISs MU-MISO OFDMA systems," *IEEE Wireless Commun. Lett.*, vol. 12, no. 2, pp. 257–261, Feb. 2023.
- [21] Z. Zhang, T. Jiang, and W. Yu, "Learning based user scheduling in reconfigurable intelligent surface assisted multiuser downlink," *IEEE J. Sel. Topics Signal Process.*, vol. 16, no. 5, pp. 1026–1039, May 2022.
- [22] A. Bansal, K. Singh, B. Clerckx, C.-P. Li, and M.-S. Alouini, "Rate-splitting multiple access for intelligent reflecting surface aided multi-user communications," *IEEE Trans. Veh. Technol.*, vol. 70, no. 9, pp. 9217–9229, Sep. 2021.

- [23] H. Fu, S. Feng, and D. W. Kwan Ng, "Resource allocation design for IRS-aided downlink MU-MISO RSMA systems," in *Proc. IEEE ICC Workshops*, 2021.
- [24] B. Zhuo, J. Gu, W. Duan, X. Gu, G. Zhang, M. Wen, and P.-H. Ho, "Partial non-orthogonal multiple access: A new perspective for RIS-aided downlink," *IEEE Wireless Commun. Lett.*, vol. 11, no. 11, pp. 2395–2399, Nov. 2022.
- [25] M. Rossanese, P. Mursia, A. Garcia-Saavedra, V. Sciancalepore, A. Asadi, and X. Costa-Perez, "Designing, building, and characterizing RF switch-based Reconfigurable Intelligent Surfaces," in *Proc. ACM WiNTECH*, 2022.
- [26] V. Jamali, G. C. Alexandropoulos, R. Schober, and H. V. Poor, "Low-to-zero-overhead IRS reconfiguration: Decoupling illumination and channel estimation," *IEEE Commun. Lett.*, vol. 26, no. 4, pp. 932–936, Apr. 2022.
- [27] Q.-U.-A. Nadeem, A. Kammoun, A. Chaaban, M. Debbah, and M.-S. Alouini, "Asymptotic max-min SINR analysis of reconfigurable intelligent surface assisted MISO systems," *IEEE Trans. Wireless Commun.*, vol. 19, no. 12, pp. 7748–7764, Dec. 2020.
- [28] X. Qian, M. Di Renzo, V. Sciancalepore, and X. Costa-Pérez, "Joint optimization of reconfigurable intelligent surfaces and dynamic metasurface antennas for massive MIMO communications," in *Proc. IEEE SAM workshop*, 2022.
- [29] S. L. Tanimoto, A. Itai, and M. Rodeh, "Some matching problems for bipartite graphs," *J. ACM*, vol. 25, no. 4, pp. 517–525, 1978.
- [30] P. Ramanathan, K. M. Sivalingam, P. Agrawal, and S. Kishore, "Dynamic resource allocation schemes during handoff for mobile multimedia wireless networks," *IEEE J. Sel. Areas Commun.*, vol. 17, no. 7, pp. 1270–1283, Jul. 1999.
- [31] R. Irmer, H. Droste, P. Marsch, M. Grieger, G. Fettweis, S. Brueck, H.-P. Mayer, L. Thiele, and V. Jungnickel, "Coordinated multipoint: Concepts, performance, and field trial results," *IEEE Commun. Mag.*, vol. 49, no. 2, pp. 102–111, Feb. 2011.
- [32] F. Guidolin, A. Orsino, L. Badia, and M. Zorzi, "Statistical analysis of non orthogonal spectrum sharing and scheduling strategies in next generation mobile networks," in *Proc. IEEE IWCMC*, 2013.
- [33] A. Marotta, D. Cassioli, C. Antonelli, K. Kondepudi, and L. Valcarenghi, "Network solutions for CoMP coordinated scheduling," *IEEE Access*, vol. 7, pp. 176 624–176 633, 2019.
- [34] S. Bassoy, M. Jaber, M. A. Imran, and P. Xiao, "Load aware self-organising user-centric dynamic CoMP clustering for 5G networks," *IEEE Access*, vol. 4, pp. 2895–2906, 2016.
- [35] F. Guidolin, L. Badia, and M. Zorzi, "A distributed clustering algorithm for coordinated multipoint in LTE networks," *IEEE Wireless Commun. Lett.*, vol. 3, no. 5, pp. 517–520, Oct. 2014.
- [36] X. Tan, Z. Sun, D. Koutsonikolas, and J. M. Jornet, "Enabling indoor mobile millimeter-wave networks based on smart reflect-arrays," in *Proc. IEEE Infocom*, 2018.
- [37] L. Anchora, L. Badia, E. Karipidis, and M. Zorzi, "Capacity gains due to orthogonal spectrum sharing in multi-operator LTE cellular networks," in *Proc. IEEE ISWCS*, 2012.
- [38] L. Rokach and O. Maimon, "Clustering methods," in *Data mining and knowledge discovery handbook*. Springer, 2005, pp. 321–352.
- [39] S. Lloyd, "Least squares quantization in PCM," *IEEE Trans. Inf. Theory*, vol. 28, no. 2, pp. 129–137, Mar. 1982.
- [40] F. Murtagh and P. Contreras, "Algorithms for hierarchical clustering: an overview," *Wiley Interdisciplinary Rev.: Data Mining Knowl. Discovery*, vol. 2, no. 1, pp. 86–97, 2012.
- [41] L. Kaufman and P. J. Rousseeuw, "Clustering by means of medoids," in *Rep. Fac. Math. Inf.*, vol. 87, no. 3, 1987.
- [42] 3GPP, "Study on channel model for frequencies from 0.5 to 100 GHz," 2020.
- [43] T. Zugno, M. Polese, N. Patriciello, B. Bojović, S. Lagen, and M. Zorzi, "Implementation of a spatial channel model for ns-3," in *Proc. ACM WNS3*, 2020.
- [44] M. Van der Laan, K. Pollard, and J. Bryan, "A new partitioning around medoids algorithm," *J. Stat. Computat. Simul.*, vol. 73, no. 8, pp. 575–584, 2003.
- [45] P. Berens, "CircStat: A MATLAB toolbox for circular statistics," *J. Stat. Softw.*, vol. 31, no. 10, p. 1–21, 2009.
- [46] V. Vasudevan and M. Ramakrishna, "A hierarchical singular value decomposition algorithm for low rank matrices," *arXiv preprint arXiv:1710.02812*, 2017.
- [47] D. Xu and Y. Tian, "A comprehensive survey of clustering algorithms," *Annals of Data Science*, vol. 2, pp. 165–193, Jun. 2015.
- [48] M. Rivera, M. Chegini, W. Jaafar, S. Alfattani, and H. Yanikomeroglu, "Optimization of quantized phase shifts for reconfigurable smart surfaces assisted communications," in *Proc. IEEE CCNC*, 2022.